Contributions of Hydroxyethyl Groups to the DNA Binding Affinities of Anthracene Probes

Michael R. Duff,[†] Willy B. Tan,[†] Akhilesh Bhambhani,[†] B. Scott Perrin, Jr.,[†] Jyotsna Thota,[†] Alison Rodger,[‡] and Challa V. Kumar*[,†]

Department of Chemistry, University of Connecticut, Storrs, Connecticut 06269-3060, and Department of Chemistry, University of Warwick, Coventry, CV4 7AL, UK

Received: June 26, 2006

Contributions of hydroxyethyl functions to the DNA binding affinities of substituted anthracenes are evaluated by calorimetry and spectroscopy. Isothermal titration calorimetry indicated that binding of the ligands to calf thymus DNA (5 mM Tris buffer, 50 mM NaCl, pH 7.2, 25 °C) is exothermic. The binding constants increased from 1.5×10^4 to 1.7×10^6 M^{-1} as a function of increase in the number of hydroxyethyl functions (0−4). DNA binding was accompanied by red-shifted absorption (~630 cm^{-1}), strong hypochromism (>65%), positive induced-circular dichroism bands, and negative linear dichroism signals. DNA binding, in general, increased the helix stabilities to a significant extent ($\Delta T_m \approx 7$ °C, $\Delta\Delta H \approx 3$ kcal/mol, $\Delta\Delta S \approx 6-20$ cal/K·mol). The binding constants showed a strong correlation with the number of hydroxyethyl groups present on the anthracene ring system. Analysis of the binding data using the hydrophobicity parameter (Log *P*) showed a poor correlation between the binding affinity and hydrophobicity. This observation was also supported by a comparison of the affinities of probes carrying *N*-ethyl ($K_b = 0.8 \times 10^5$ M^{-1}) versus *N*-hydroxyethyl side chains ($K_b = 5.5 \times 10^5$ M^{-1}). These are the very first examples of a strong quantitative correlation between the DNA binding affinity of a probe and the number of hydroxyethyl groups present on the probe. These quantitative findings are useful in the rational design of new ligands for high-affinity binding to DNA.

Introduction

A better understanding of DNA−ligand interactions is essential for the rational design of ligands to influence key biological processes such as gene expression, transcription, or translation.[1] Although hydrogen-bonding groups are known to play a key role in these interactions,[2] quantitative data on their contributions are still sparse.[3] One approach is to systematically increase the number of potential H-bonding side chains on a ligand and quantify their contributions to the DNA binding affinities.[4] Focus of the current investigations is to quantify the interactions of hydroxyethyl side chains by calorimetric and spectroscopic studies.

Anthracene derivatives are chosen, in the current investigations, for the following reasons. Several anthracene derivatives are known to have significant biological activities against specific types of cancers.[5] Pseudourea, for example, was one of the earliest examples of anthracene-based drugs tested in clinical trials,[6] and anthracene itself was reported to be effective against specific skin ailments.[7] The planar, linear, three-ring system of the anthracene nucleus has potential for significant overlap with the DNA base pairs, and it is expected to facilitate intercalation of the probe into the DNA helix (Chart 1).[8] The versatile chemistry of anthracene nucleus provides a convenient route to prepare a number of closely related derivatives.[9]

Additional advantages of the anthracene probes are that: (1) they have moderate absorption cross-sections in the near-UV region and good fluorescence quantum yields, which are useful to monitor ligand binding to DNA by spectroscopic methods;[10] (2) while the GC sequences of DNA quench the fluorescence of most anthracene derivatives, AT sequences enhance anthryl fluorescence, and this provides a useful marker to identify the nature of the binding site;[11] (3) anthryl probes have long-lived triplet excited states, which can be used to induce significant DNA damage and strand cleavage;[12,13] (4) substituents at the 9 and 10 positions of the anthracene nucleus are strategically positioned such that these occupy the grooves when the anthracene moiety is intercalated into the helix;[14] and (5) the spectroscopic signatures of the DNA binding modes of anthracene probes have been recently identified,[15] and these will be useful in the analysis of the current data.

CHART 1: Two Major Binding Modes (Intercalation and Groove Binding) of Anthryl Ligands to the DNA Double Helix[a]

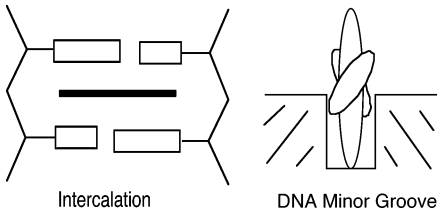

[a] Only one geometry for the minor groove binding is shown, and the small ovals in the front and the back of the large oval represent the 9,10-substituents on the anthracene ring.

The number of hydroxyethyl substituents on the anthracene nucleus is increased from 0 to 4 by substitution at the 9 and 10 positions (**1**−**4**, Chart 2). The hydroxyethyl side chain is chosen for these studies due to its ability to support potential hydrogen-bonding contacts with the helix. These functions have been implicated in enhanced binding affinities of some metal complexes and anticancer agents.[5b,16] However, there are no clear, quantitative correlations between the DNA binding affinities and the number of such functions present on the ligand.

* Corresponding author. E-mail: challa.kumar@uconn.edu.
[†] University of Connecticut.
[‡] University of Warwick.

10.1021/jp063997m CCC: $33.50
Published on Web 09/22/2006

CHART 2: Structures of the Anthracene Derivatives Discussed in This Study

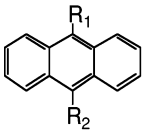

#		R_1	R_2
1.	AMAC	$CH_2NH_3^+$	H
2.	MEA	$CH_2NH_2^+CH_2CH_2OH$	H
3.	BMEA	$CH_2NH_2^+CH_2CH_2OH$	$CH_2NH_2^+CH_2CH_2OH$
4.	BDEA	$CH_2NH^+(CH_2CH_2OH)_2$	$CH_2NH^+(CH_2CH_2OH)_2$
5.	APAC	$CH_2CH_2CH_2NH_3^+$	H
6.	N-Et-AMAC	$CH_2NH_2^+CH_2CH_3$	H

The hydroxyethyl group is similar in size, flexibility, conformation, and polarity to the propylamine side chain of **5**, and the latter was suggested to make H-bonding contacts with the DNA minor groove.[14] However, the OH groups of **2**−**4** are positioned one covalent bond farther away from the anthryl ring than the NH_2 group of **5**, and this feature is expected to allow higher flexibility for the side chain.

Among the probes shown in Chart 2, probes **1** and **4** indicated enhanced binding affinity with **4** when compared to that of **1**.[10,14,15] However, it is not clear if this increased affinity is due to the increased number of hydroxyethyl functions or due to increased hydrophobicity of the probe. Anthracene derivatives **2** and **3** were prepared, therefore, and they have been examined to evaluate the role of the side chains in the binding interaction. By comparing the binding properties of **1**−**4**, it is possible to evaluate the contributions of these side chains to the overall binding affinity. Comparison of the binding properties of **2** with those of **6** would reveal the contributions of the OH group to the binding interactions. Quantitative data on the binding of these probes to calf thymus DNA are presented here, and these indicate a strong correlation between the number of hydroxyethyl functions present on the probe and their binding affinities. Such correlations are useful for the rational design of ligands of high DNA binding affinities.

Experimental Section

DNA Samples. Calf thymus DNA (CT DNA, type I) was purchased from Sigma Chemical Co. (St. Louis, MO) and purified according to published protocols.[17] All experiments were carried out in Tris buffer (5 mM Tris, 50 mM NaCl, pH adjusted to 7.2), unless mentioned otherwise. Stock solutions of CT DNA were prepared by dissolving an appropriate mass of DNA in Tris buffer. All DNA concentrations are expressed in terms of base pairs of DNA.

Synthesis of 9-(*N*-(2-Hydroxyethyl)aminomethyl)anthracene (MEA, 2). A solution of 9-chloromethylanthracene (50 mg, 0.22 mmol) in THF (15 mL) was added to a solution of ethanolamine (61 mg, 1 equiv, 10 mL of THF) over a period of 0.5 h. The reaction was allowed to proceed for 24 h, and progress was checked by monitoring the absorption spectrum of the reaction mixture. Disappearance of the 397 nm absorption peak due to the 9-chloromethylanthracene was noted, which was accompanied by the gradual growth of the product band at 388 nm. The reaction mixture was filtered, concentrated under vacuum, and allowed to crystallize. The crude product was further purified by crystallization from methanol, in 54% yield, mp 116−119 °C, and the melting point matched with the reported value.[18] ^{1}H NMR (CH_3OD) ppm: 8.43 (s, 1), 8.35 (d, 2), 8.00 (d, 2), 7.52 (t, 2), 7.44 (t, 2), 4.71 (s, 3), 3.69 (m, 2), 2.93 (m, 2). Mass spectrum indicated a molecular ion peak at (*m*/*z*) 252.

Synthesis of 9,10-Bis(*N*,*N*-(2-hydroxyethyl)aminomethyl)-anthracene (BMEA, 3). A solution of 9,10-bisbromomethylanthracene in THF was added to excess ethanolamine (2.1 equiv in THF). Reaction with the bromo-derivative was faster than with the chloro-derivative described above, and the former resulted in cleaner reactions. The product was crystallized from methanol in 23% yield, mp 157−160 °C, and the melting point matched with the reported value.[19] ^{1}H NMR (CH_3OD) ppm: 8.45 (m, 4), 7.65 (m, 4), 5.03 (s, 2), 3.81 (t, 4), 3.14 (t, 4). Mass spectrum indicated a molecular ion peak at (*m*/*z*) 325.

Even though it is appropriate to refer to these ligands by the numbers shown in Chart 2, it is more convenient to use the corresponding acronyms, and these are used from this point on in this Article.

Isothermal Titration Calorimetry (ITC). ITC studies were performed on a MicroCal VP-ITC microcalorimeter (MicroCal Inc., Northampton, MA). Anthryl derivative (∼350−170 μM) was titrated into CT DNA (100 μM DNA, Tris buffer). Multiple injections of 8−16 μL of ligand solution into a solution of CT DNA (1.4167 mL) were carried out at specific intervals, until the binding was saturated. Samples were allowed to equilibrate between injections. The entire experiment was controlled by software supplied by MicroCal, Inc., and the data were fit using the Origin 5.0 software package. Multiple data sets were acquired and analyzed using eq 1. Analysis with different starting values resulted in a consistent set of parameters, which are within our experimental error.

$$Q = 0.5(nM_t\Delta HV_o)[1 + (X_t/nM_t) + (1/nK_bM_t) - \sqrt{[(1 + (X_t/nM_t) + (1/nK_bM_t))^2 - 4X_t/nM_t]}] \quad (1)$$

The heat released (Q) during the titration is related to the molar heat of ligand binding (ΔH), volume of the sample cell (V_o), the bulk concentration of the ligand (X_t), concentration of DNA (M_t), the intrinsic binding constant (K_b), and the number of binding sites (n) by eq 1. The above equation was derived from basic thermodynamic principles, under equilibrium conditions.[20] Thermodynamic parameters for the binding such as ΔH, ΔS, binding constant (K_b), and the binding site size (n) are calculated directly from the ITC data.

Absorption Studies. Absorption spectra were recorded on a diode array HP 5750 spectrophotometer. A solution of the anthryl probe (11 μM MEA or 12 μM BMEA, 1 mL, Tris buffer, in a 1-cm path length cuvette) was titrated by adding 5 μL increments of CT DNA (3−6 mM, Tris buffer), while monitoring the absorbance in 300−500 nm region. The total volume of CT DNA added during the titration did not exceed 10% of the starting volume, and the data have been corrected for volume changes. The absorption data were analyzed using Scatchard eq 2 to estimate the binding constants.

$$1/C_f = K_bn(1/r) - K_b \quad (2)$$

In eq 2, C_f is the concentration of the free probe, n is the binding density, and r is the ratio of concentration of bound probe (C_b) to that of DNA. The absorbance data are used to calculate C_f by using the relations $C_f = (A_{obs} - \epsilon_bC_t)/(\epsilon_f - \epsilon_b)$, where A_{obs} is the absorbance at the peak position of the probe−DNA mixture, C_t is the total concentration of the probe, while ϵ_f and ϵ_b are the extinction coefficients of the free and bound probes, respectively. The value of ϵ_b was estimated from a plot of A_{obs} versus 1/[DNA]. In cases where A_{obs} versus 1/[DNA] plot was not linear, the absorption spectrum of the probe was obtained from a mixture of probe and a high concentration of CT DNA (1 mM). The intrinsic binding constant (K_b) was estimated from these data by plotting $1/C_f$ versus $1/r$ and by fitting the data to eq 1. Alternatively, the data were also analyzed using the McGhee and von Hippel eq 3 for comparison.[21]

$$r/c_f = K_b(1 - nr)[(1 - nr)/[1 - (n - 1)r]]^{n-1} \quad (3)$$

The percent hypochromism was determined from the estimated values of ϵ_f and ϵ_b. The free energy of the binding ($\Delta G°$) was calculated from eq 4.

$$\Delta G° = -RT \ln K_b \quad (4)$$

Induced Circular Dichroism (CD) Studies. The CD spectra were recorded on a Jasco J-710 spectropolarimeter (Jasco Inc., Easton, MD) interfaced with an IBM-PC computer. A mixture of the probe (75 μM) and CT DNA (300 μM) solutions was placed in a quartz cuvette of 1-cm path length, for recording the spectra in the 325−425 nm window. A cuvette of 2-mm path length was used for recording the CD spectra in the 200−325 nm window. Parameters of 1 nm bandwidth, 20 mdeg sensitivity, and 4 s response time were used to record the spectra.

Linear Dichroism Studies. Flow linear dichroism (LD) spectra were recorded on a Jasco J-715 spectropolarimeter adapted for LD measurements by using a cylindrical flow cell. The flow is generated by the rotation of an inner quartz cylinder, spaced 0.5 mm from a stationary steel/quartz cylinder.[22] Light from the source passes through the center of the cell and through the solution. The ratio of the concentration of DNA to that of the probe was varied at each stage by adding ligand solution, as well as an appropriate volume of DNA solution, so that the DNA concentration (and hence the sample viscosity) is constant. All LD spectra were measured at pH = 6.9 (1 mM sodium cacodylate, 50 mM NaCl).

DNA Melting Experiments. DNA melting studies were carried out on a Hewlett-Packard 8452A diode array spectrophotometer equipped with an HP 89090A peltier thermostat, controlled by an HP Vectra 386/16N computer. The helix melting temperatures were measured by monitoring the sample absorbance at 270 nm (Tris buffer).

Differential Scanning Calorimetry. The DSC experiments were performed on a model 6100 Nano-II differential scanning calorimeter from Calorimetry Sciences Corporation (Lindon, UT). The calorimeter had a cell volume of 0.299 mL, and it was interfaced with a Dell personal computer and controlled by software supplied by the manufacturer. In a series of DSC scans, both of the cells were first loaded with Tris buffer (5 mM Tris, 25 mM NaCl, pH 7.2), equilibrated at 10 °C for 10 min, and then the temperature was raised from 10 to 100 °C at a scan rate of 2 °C/min. The buffer versus buffer scan was repeated once more, and, after cooling to room temperature, the sample cell was emptied, rinsed, and loaded with the sample.

The samples and reference solutions were degassed for at least 5 min at room temperature and carefully loaded into the cells to avoid bubbles. During the scans, constant pressure of 3 atm was maintained over the solutions to prevent possible degassing of the samples during heating. A background scan, recorded with the buffer in both cells, was subtracted from each test scan. A typical example consisted of a scan of CT DNA (60 μM, Tris buffer) in the presence or absence of the probe (33 μM) from 10 to 100 °C, at a heating rate of 2 °C/min.

The excess molar heat capacity (C_p) was calculated from the raw data, using the mean molecular mass of 330 g/mol of nucleotides, and the partial specific volume of CT DNA has been calculated to be 0.54 mL/g.[23] Thermodynamic parameters of the helix denaturation were calculated, and reported values are averages of at least three measurements.

Sonication of CT DNA. Sonicated CT DNA was prepared by following a reported procedure.[24] A 50 W Cole-Parmer ultrasonic processor equipped with a 3 mm titanium microtip was used to sonicate the DNA sample. CT DNA (40 mL, ∼1 mg/mL, Tris buffer) was placed in a plastic test tube, cooled in an ice bath, and nitrogen gas bubbled through the DNA solution for 15 min. The solution was sonicated for 5 min followed by purging with nitrogen for 5 min. This cycle was repeated 30 times, and, after the 30th time, the solution was purged with nitrogen for 15 min. The DNA solution was again sonicated for a total of 330 s (10 s sonication followed by 5 min purging with nitrogen), and the solution was dialyzed five times against Tris buffer. The average molecular weight of DNA was estimated by measuring viscosity, using eq 5.[24] The intrinsic viscosity, [η], was 1.96 dL g^{-1}, and the average molecular weight of sonicated DNA has been estimated to be 3.0×10^5 Da. The sonicated DNA sample had a A_{260nm}/A_{280nm} ratio of 1.83, and the melting temperature of sonicated CT DNA matched with that of the unsonicated sample. Hyperchromicity (H, eq 6, where $A_{25°C}$ and $A_{96°C}$ are absorbances at 25 and 96 °C, respectively) of the sonicated DNA solution was comparable to that of the unsonicated sample.

$$[\eta] = 1.45 \times 10^{-6}\, M^{1.12} \quad (5)$$

$$H = (A_{96°C} - A_{25°C})/A_{25°C} \quad (6)$$

Computational Modeling. Selected properties of the anthracene probes were calculated by Computer Aided Chemistry (CAChe v. 4.9, Fujitsu Inc.), running on a Blue and White G3/G4 Apple Macintosh computer. The partition coefficient for the octanol/water system was calculated with ClogP package of CAChe.

Results and Discussion

Anthracene derivatives are investigated for their interaction with DNA by calorimetric, spectroscopic, and computational studies. These show a strong role of hydroxyethyl side chains in the binding interaction. First, the binding data are presented, and these are followed by characterization studies.

ITC Studies. Titration of a solution of MEA (**2**) into a solution of CT DNA indicated exothermic binding (Figure 1A), and addition of the ligand solution to DNA resulted in prompt heat release. Binding was saturated when the ratio of the concentration of the probe to that of DNA exceeded 0.5. Titration of the ligand into buffer (no DNA) indicated small, exothermic heat of dilution (top curve, Figure 1A). Dilution of CT DNA with buffer resulted in negligible heat release (data not shown).

The area under each peak of the ITC titration data was integrated, and the heats of dilution were subtracted. The net heat released during the titration was plotted as a function of [MEA]/[CT DNA] (Figure 1B), and the data have been fitted to a single-binding-site model (solid line, eq 1). Calculations using different initial values converged to the same set of binding parameters, consistently, and the corresponding binding parameters are collected in Table 1.

The enthalpy of binding of MEA, estimated from the above data, is -3.4 ± 1.5 kcal/mol, and exothermic binding of similar anthracene derivatives to CT DNA has been reported.[25] The best fit to the data indicated a binding constant of $(3.7 \pm 1.5) \times 10^5$ M^{-1}, and this value is an order of magnitude greater than the corresponding binding constants of AMAC, APAC, or N-Et-AMAC with CT DNA.[14] Note that these were measured under the same conditions of buffer and ionic strength. MEA differs from N-Et-AMAC in terms of the single OH group in the side chain, and hence the enhanced affinity of MEA is most likely due to the additional OH group in this probe. Note that the pK_a values of these two probes are expected to be similar (pK_a of MEA = 6.6 ± 0.3), and both ligands are expected to

TABLE 1: Thermodynamic Parameters Obtained for the Binding of Anthryl Probes to CT DNA from ITC Measurements (Tris Buffer, 298 K)

ligand	*n*	K_b (M^{-1})	ΔH (kcal/mol)	ΔS (cal/mol·K)	ΔG (kcal/mol)
N-Et-AMAC			0		
MEA	0.22 ± 0.08	$(3.7 \pm 1.5) \times 10^5$	-3.4 ± 1.5	1.5 ± 17	-7.2 ± 0.3
BMEA	0.15 ± 0.01	$(1.7 \pm 0.4) \times 10^5$	-5.5 ± 1.9	5.3 ± 6.3	-7.1 ± 0.2

be protonated to a similar extent, under the experimental conditions.

The above analysis also indicated that the binding site size ($1/n$) for MEA is ~4 base pairs, and this value is greater than what is anticipated from the neighbor exclusion principle.[14] Analysis of the data with smaller binding site sizes did not give good fits and hence is not valid.

Similar to the exothermic binding of MEA, titration of BMEA (169 μM) into CT DNA (100 μM) also indicated strong heat release (Figure 2A). Binding saturated at a ratio of probe to DNA concentrations of >0.35. Subtraction of the corresponding heats of dilution and subsequent analysis of the data indicated that the enthalpy of binding of BMEA is -5.5 ± 1.9 kcal/mol. This value is greater than that of MEA, or other anthracene probes reported earlier.[15] Analysis of the BMEA binding isotherm, as in the case of MEA, by single-binding-site model resulted in satisfactory fits to the data (Figure 2B), and these indicated a binding constant of $(1.7 \pm 0.4) \times 10^5$ M^{-1}. Note that ITC analysis indicates that the affinity of BMEA is smaller than that of MEA, but these values are nearly within experimental error.

Absorption Studies. The absorption spectra of MEA and BMEA (300−420 nm) undergo significant changes on binding to CT DNA, and these provided a convenient handle to characterize their interactions (Figure 3A,B). The absorption spectra of the probes were recorded in the presence of increasing concentrations of DNA, and the spectra have been corrected for small changes in volume during the titration. The extinction coefficients of the bound chromophore were determined from the *y*-intercepts of the half reciprocal plots of absorbance versus 1/[DNA] (Table 2).

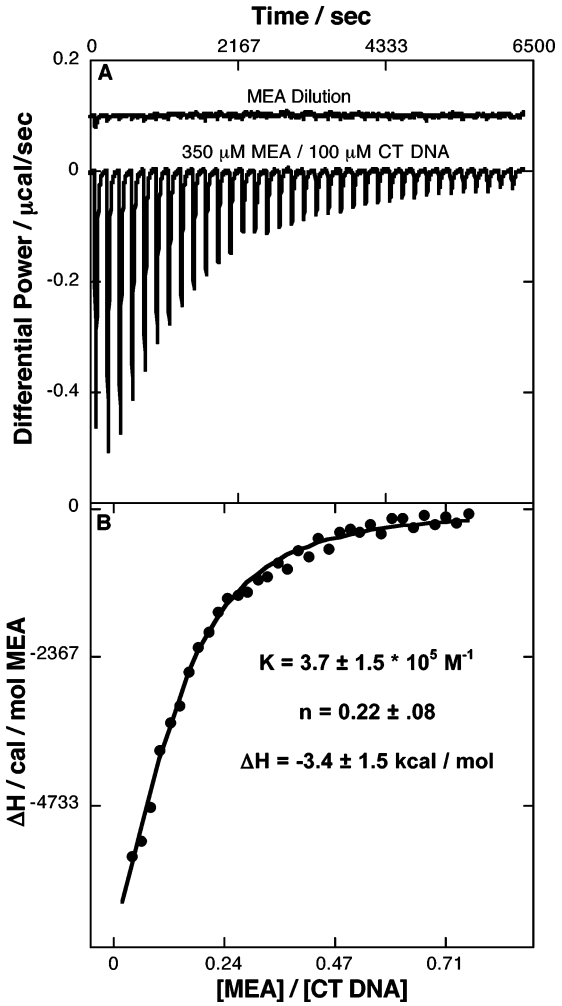

Figure 1. Isothermal titration calorimetry data for the binding of MEA (350 μM) to CT DNA (100 μM, 5 mM Tris, 50 mM NaCl, pH 7.2, 25 °C). (A) Heat released during the titration of CT DNA (100 μM) by successive additions of a concentrated solution of MEA (350 μM). The heat released during the dilution of MEA (no DNA) is shown separately. (B) The MEA/DNA binding isotherm from Figure 1A data; the solid line represents a fit according to the single binding site model.

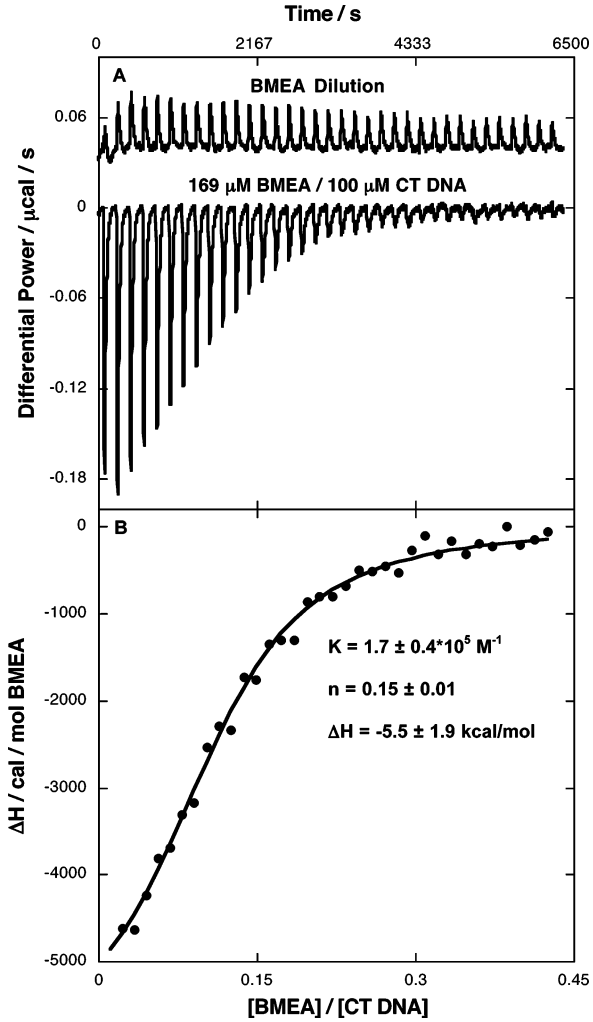

Figure 2. The isothermal titration calorimetric data for the binding of BMEA to CT DNA. (A) The heat released (top) when a concentrated solution of BMEA (169 μM) was titrated into a solution of CT DNA (100 μM, 5 mM Tris, 50 mM NaCl, pH 7.2, 25 °C). (B) The BMEA/CT DNA binding isotherm, where the solid line represents the best fit to the data, according to the single binding site model.

TABLE 2: Spectroscopic Data Obtained for the Probe/CT DNA Mixtures (Tris Buffer, 298 K)

probe	isosbestic points (nm)	λ_{max} free (nm)	λ_{max} bound (nm)	ΔE (cm^{-1})	%hypochromism (@ nm)	ϵ_{free} (M^{-1} cm^{-1}) (@ nm)	ϵ_{bound} (M^{-1} cm^{-1}) (@ nm)
MEA	394	387	396	650	67 (387)	6100 (367)	1700 (367)
BMEA	400, 384	394	404	630	76 (394)	6940 (373)	1800 (373)

The MEA/CT DNA absorption titrations, for example, indicated extensive broadening in the 300−420 nm region and a significant red shift (650 cm^{-1}). Absorbance at 394 nm was independent of the DNA concentration (isosbestic point), and the presence of the isosbestic point clearly indicates the smooth conversion of one chromophore to another (free and bound) as the titration progressed. The area under the absorption curve was drastically reduced (hypochromism) in the presence of excess of DNA, and the extent of hypochromism at 387 nm, for example, was 67% (Table 2). Such large hypochromism values were also noted when anthracene derivatives are intercalated in the helix.[14]

Similar to MEA, the absorption spectra of BMEA (12 μM) were recorded in the presence of increasing concentrations of CT DNA (0−132 μM) (Figure 3B), and these also indicated red-shifted (630 cm^{-1}) maxima as well as large hypochromism (76% @ 394 nm). Clear isosbestic points at 400 and 384 nm are also evident from the spectra. Note that the vibronic bands of BMEA/CT DNA are broadened extensively but they are clearly resolved, unlike in the case of MEA/CT DNA (Figure 3A).

The large hypochromism values and large red shifts are attributed to a strong electronic interaction between the π-electrons of the probe and those of the DNA bases.[26] The magnitude of hypochromism is expected to depend inversely on the distance of separation between the ligand and the nucleobases as well as the relative orientations of the interacting moieties.[27] The strengths of these electronic interactions of MEA and BMEA with DNA are comparable to those of APAC and N-Et-AMAC. The absorption characteristics of the anthracene probes, such as the above, have been assigned to the intercalative binding of anthracene probes (Chart 1).[15] On the basis of these reports, we suspect that MEA and BMEA also intercalate into the helix.

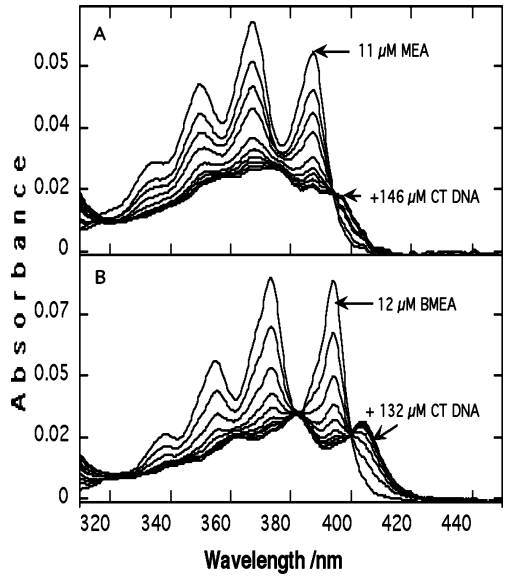

Figure 3. Absorption spectra of MEA and BMEA in the presence of increasing concentrations of CT DNA (5 mM Tris, 50 mM NaCl, pH 7.2, 25 °C): (A) MEA (11 μM) in the presence of CT DNA (0−146 μM), and (B) BMEA (12 μM) in the presence of CT DNA (0−132 μM).

TABLE 3: Intrinsic Binding Constants Estimated from the Absorption Titrations (Tris Buffer, 298 K)

probe	K_b (10^5 M^{-1})[a]	$\Delta G°$ (kJ/mol)[a]	K_b (10^5 M^{-1})[b]	$\Delta G°$ (kJ/mol)[b]
N-ET-AMA C	0.8 ± 0.05	-24 ± 1.0	0.12 ± 0.001	-23 ± 0.1
MEA	5.5 ± 0.1	-33 ± 0.1	1.0 ± 0.01	-28 ± 0.1
BMEA	8.0 ± 1.3	-34 ± 0.5	2.0 ± 0.01	-30 ± 0.1

[a] From Scatchard plot. [b] From von Hippel plot.

Intrinsic Binding Constants. The absorption titration data were analyzed to estimate the corresponding binding constants by using the Scatchard equation (eq 2). Binding isotherms were constructed from these data (Figure 4), and best linear fits to the data resulted in binding constants of 5.5×10^5 and 8.0×10^5 M^{-1} for MEA and BMEA, respectively. As an alternative to Scatchard analysis, the data were also analyzed using the McGhee and von Hippel eq 3.[21] All of the corresponding binding parameters are collected in Table 3.

Note that Scatchard analysis gave higher binding constants than von Hippel plots, but both indicated the same trends. According to both models, the binding constant of BMEA is larger than that of MEA, and at first sight this may appear to be due to higher charge on BMEA than MEA. The pK_a of $MEAH^+$ is 6.6 ± 0.3, and this value is expected to be comparable to the corresponding second pK_a of $BMEA(2H)^{2+}$. The first pK_a of $BMEA(2H)^{2+}$ is 5.9 ± 0.3, and the second amino group is unlikely to be protonated at pH 7.2.[28] Therefore, BMEA would not exist as a dicationic species at pH 7.2, and a significant fraction of both probes will be singly protonated. Therefore, the greater binding affinity of BMEA over MEA or that of MEA over N-Et-AMAC cannot be explained by their pK_a values. Note also that the binding affinities obtained from ITC are in reasonable agreement with

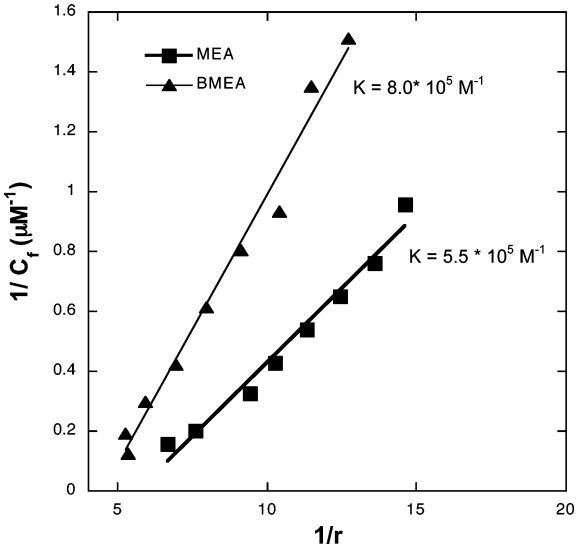

Figure 4. The binding isotherms for the anthracene probes (5 μM) with CT DNA (0−75 μM, 5 mM Tris, 50 mM NaCl, pH 7.2, 25 °C).

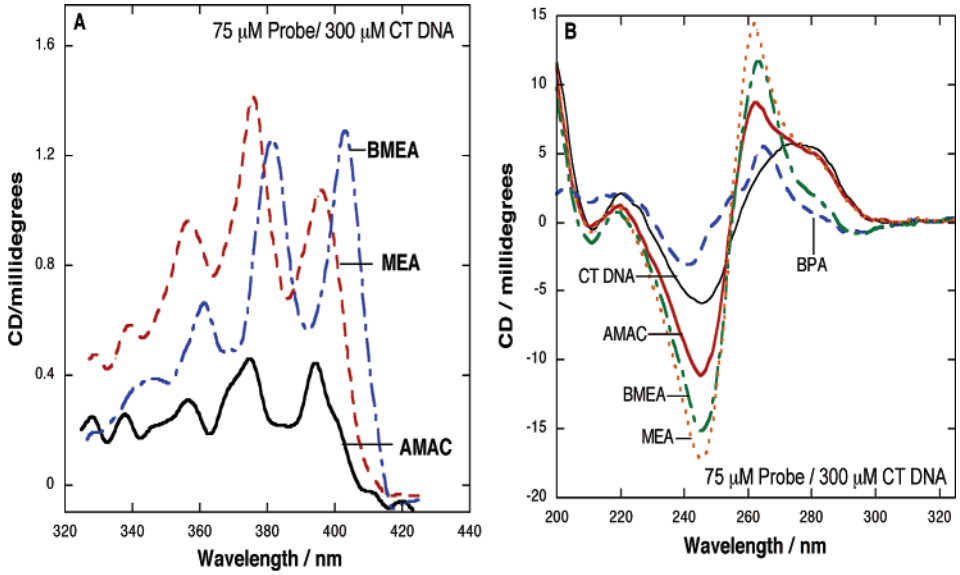

Figure 5. Induced circular dichroism spectra of the anthracene probes (75 μM) recorded in the presence of CT DNA (300 μM) (5 mM Tris, 50 mM NaCl, pH 7.2) in the near-UV region (A) and the UV region (B).

TABLE 4: Peak Positions of the ICD Spectra (Tris Buffer, 298 K)

probe	ICD peaks (nm)	UV−vis peaks (bound, nm)
MEA	398, 377, 358	very broad
BMEA	403, 381, 360	404, 382, 361

those of the absorption measurements but the latter are more accurate. The binding affinity data clearly illustrate the role of the side chains in controlling the overall affinities of the anthracene derivatives.

Induced Circular Dichroism (ICD) Studies. Binding of anthracene probes to DNA results in induced circular dichroism, and the ICD spectra indicate the orientation of the chromophore relative to the base pair dyad axis.[29] Positive ICD peaks are expected in the 320−400 nm region when the anthryl short axis is oriented perpendicular to the helix axis.[30]

Both MEA and BMEA showed positive ICD signals upon binding to DNA (Figure 5A), and these are consistent with the positive ICD spectra observed with other anthracene intercalators, including **1**, **4**, **5**, and **6**.[14] Note that the ICD peak positions of MEA and BMEA match with the absorption peak positions of the bound probes (Table 4), and these indicate that the ICD peaks correspond to the same chromophore that is responsible for the red-shifted absorption spectra in Figure 3.

In addition to the anthryl ICD data, the DNA CD at 280 nm is also an indicator of the probe binding modes. Unwinding of the DNA helix by classical intercalators, for example, results in strong decreases in the intensity of the 280 nm band.[31] Note that anthryl probes do not have a significant absorption in this region, and the contributions of any ICD signals in this region are negligible. The CD spectra in the 260−300 nm region are essentially due to the nucleobases. The intensity of the DNA CD at 280 nm is substantially reduced by BMEA (Figure 5B), and this observation is a strong indicator of classical intercalation. Similar to BMEA, a large reduction in 280 nm CD was also noted with another anthracene probe, BPA (R_1═R_2═CH_2− piperidine), and this reduction has been assigned to the classical intercalation of BPA.[15] In contrast to the behavior of these two probes, MEA did not cause such decreases in the 280 nm CD, and MEA may bind via partial intercalation. This is because the absorption spectral changes noted for MEA (Figure 3A) are not consistent with groove binding. Groove binding of anthracene probes did not produce any red-shifts in the absorption spectra.[15] Therefore, the two anthryl probes show specific differences in terms of their interaction with CT DNA.

Linear Dichroism Studies (LD). The above assignments of the binding modes are confirmed in LD studies. LD spectroscopy is an excellent tool to examine the orientations of chromophores bound to the DNA helix. The absorption transitions of the anthryl probes in the 320−400 nm region are short-axis polarized, while the 252 nm transition is long-axis polarized.[32] Classical intercalation of the probe results in both the long and the short axes of the probe oriented perpendicular to the helix axis, and this should give rise to negative LD signals at both absorption regions (∼252 and 320−400 nm). This was indeed observed at low loading of MEA and BMEA. The ligand LD at 252 nm is overlaid on the negative signal due to the DNA bases.

At low loadings, the LD spectra of the probes show negative peaks in the 252 and 320−400 nm regions (Figure 6). At high loadings, a small dip at 257 nm and negative LD in 320−400 nm region are noted. The spectra suggest intercalation of these probes. Intercalators usually stiffen the DNA, and that should lead to a larger DNA LD signal at 280 nm (anthrylene probes do not absorb in this region). LD data of a range of ligands suggest that major groove bound molecules tend to bend DNA, thus reducing the DNA LD, whereas the minor groove bound ligands stiffen the DNA.[33]

A comparison of the degree of change of the LD at the 257 (or 280) nm region indicates the differences in the binding modes of the probes. MEA significantly stiffens the DNA and has a small dip at 257 nm, appearing at DNA base:ligand ratios $< \sim$2.5:1. This small positive dip at 257 nm is assigned to a nonintercalative binding mode in which the anthracene long axis is less than 54.7° from the helix axis, perhaps stacking on the outside of the helix, or lying along a groove. It is important to note that this feature disappears when excess of DNA is present in the solution. BMEA also stiffens the DNA in a similar manner. The dominant binding mode for MEA can be concluded to be intercalation with its tail lying down the minor groove. The same is perhaps true for BMEA, although it has one side chain in each groove. Thus, the LD data lend strong support to the above conclusions.

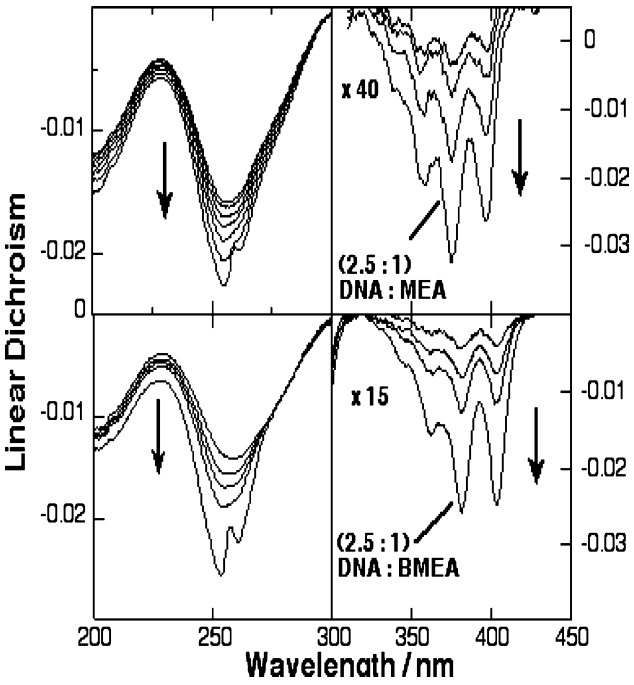

Figure 6. Linear dichroism spectra of CT DNA recorded in the presence of increasing concentrations of MEA and BMEA (1 mM sodium cacodylate, 50 mM NaCl, pH 6.9). In each set, the top spectra were obtained with CT DNA (160 μM CT DNA, no probe). Increments of the probe solutions were continually added to give decreasing ratios of DNA:probe concentrations (from 80:1 to 2.5:1) while keeping the DNA concentration constant by the addition of appropriate amounts of DNA solutions.

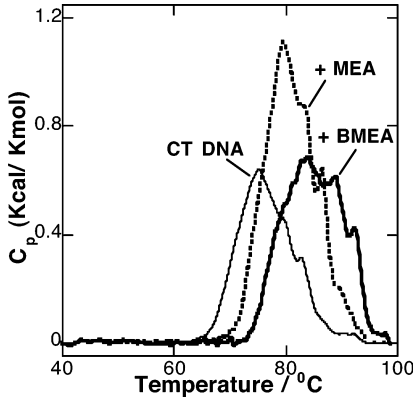

Figure 7. The differential scanning calorimetric thermograms of CT DNA (60 μM, thin line) and mixtures of the ligand/DNA complexes (5 mM Tris, 25 mM NaCl, pH 7.2). Significant improvements in the helix denaturation temperatures due to MEA (33 μM, dashed line) and BMEA (36 μM, thick line) are clear from the thermograms. The corresponding thermodynamic parameters are collected in Table 5.

DSC Studies. The thermodynamic characteristics of the helix denaturation were quantified by DSC studies. The DSC thermogram of CT DNA (60 μM) is shown in Figure 7 (thin line), which matches with the reported thermogram.[34] The helix denaturation is endothermic, and the DSC profile indicates one major transition around 75 °C as well as several minor transitions or satellite peaks. The satellite peaks are attributed to highly repetitive short base pair stretches of GC sequences, which denature at higher temperatures than other stretches of DNA.[34−36] Multiple DSC transitions of CT DNA are related to the heterogeneity of its base composition along the helix.[37]

The enthalpy change (ΔH) associated with the thermal denaturation is the integrated area under the DSC curve, and ΔH is model independent. On the other hand, ΔS was calculated assuming that the transition is reversible, and this assumption is valid/accepted in the literature.[36] Because of the heterogeneous nature of the base sequence in CT DNA, the renaturation of the single-stranded CT DNA is kinetically slow and not reversible on the DSC time scales. Even so, it is common to treat this transition as reversible and extract the corresponding thermodynamic parameters. The values thus obtained for CT DNA, from our data, are $T_m = 75.2$ °C, $\Delta H = 7.6 \pm 0.5$ kcal/mol, and $\Delta S = 22 \pm 5$ cal/mol·K (Table 5). These are in good agreement with the literature.[36]

TABLE 5: Thermodynamic Parameters Obtained for the Thermal Denaturation of CT DNA (60 μM), in the Absence and in the Presence of MEA (33 μM) or BMEA (36 μM) (Tris Buffer)

ligand	T_m (°C)	ΔH (kcal/mol)	ΔS (cal/mol·K)
CT DNA	75.2 ± 0.2	7.6 ± 0.5	22 ± 5
MEA	79.1 ± 0.1	11.2 ± 0.3	40 ± 5
BMEA	83.5 ± 0.7	10.0 ± 0.7	28 ± 2

Next, we examined the thermal denaturation profile of a mixture of MEA (33 μM) and CT DNA (60 μM) to further characterize the binding interactions. The data indicated an endothermic transition similar to that of CT DNA, but the profile is shifted to higher temperatures. Note that the satellite peaks are also shifted to higher temperatures in a corresponding manner. The enthalpy of denaturation of MEA/CT DNA estimated from these data (11.2 ± 0.3 kcal/mol) is significantly greater than that of CT DNA (7.6 ± 0.5 kcal/mol, Table 5). The helix stability, therefore, is increased by 3.6 ± 0.5 kcal/mol by the binding of MEA. Note that the extent of helix stabilization noted here is substantive and beyond the experimental error.

The DSC studies of BMEA/DNA mixture also indicated substantive changes in the DSC thermograms and increments in T_m (Figure 7A, Table 5). The helix stability is enhanced by 2.4 ± 0.5 kcal/mol, which is comparable to that observed with MEA. Note that similar increases in the ΔH values are also noted with other ligands.[25] Such stabilization was only noted with anthracene intercalators, while groove binding of anthracene ligands did not stabilize the helix.[15,38] Even though both intercalators as well as groove binders are known to improve helix stability, in the case of anthracene probes only intercalators show substantial improvements in helix stability.[15]

In addition to the above DSC studies, we also examined the influence of buffer characteristics on the above thermodynamic parameters. For example, the temperature coefficient of the pK_a of Tris buffer is substantial, while that of citrate is near zero.[39] We examined, therefore, the influence of buffer cations by using three buffers, while maintaining the same ionic strength. The thermodynamic parameters estimated for the denaturation of CT DNA in specific buffers showed measurable differences (Table 6). Despite these differences, the presence of BMEA resulted in similar increments in the T_m, ΔH, and ΔS values of CT DNA (Table 6). Therefore, the temperature dependence of the pK_a values of the buffer did not influence the helix stabilization endowed by BMEA.

The influence of the length of DNA helix on these parameters is also investigated by replacing the highly polymerized CT DNA by sonicated CT DNA. To minimize any buffer effects, the DSC data were collected with citrate buffer. The sonicated CT DNA did not show any differences from that of the intact CT DNA (Supporting Information). The corresponding thermodynamic parameters are collected in Table 6. These show that sonication of CT DNA did not have a significant effect on

TABLE 6: Thermodynamic Parameters Obtained for the Thermal Denaturation of CT DNA in the Presence and in the Absence of BMEA in Three Different Buffers (Citrate Buffer, 5 mM sodium citrate, 0.44 mM NaCl, pH 7.2; Tris Buffer, 5 mM Tris HCl, 25 mM NaCl, pH 7.2; and Phosphate Buffer, 10 mM Dibasic Potassium Phosphate, 7 mM NaCl, pH 7.2)

ligand	buffer	T_m/°C	ΔH (kcal/mol)	ΔS (cal/mol·K)
CT DNA	phosphate	72.9 ± 0.3	8.1 ± 0.4	23 ± 2
CT DNA/BMEA	phosphate	81.3 ± 0.8	8.6 ± 0.5	25 ± 3
CT DNA	citrate	67.6 ± 0.4	8.7 ± 0.8	26 ± 4
CT DNA/BMEA	citrate	76.3 ± 1.6	7.8 ± 1.1	23 ± 6
CT DNA (sonicated)	citrate	67.6 ± 0.3	8.3 ± 0.7	22 ± 4
CT DNA (sonicated)/ BMEA	citrate	76.2 ± 1.1	7.9 ± 0.6	23 ± 5

the denaturation thermodynamics of CT DNA, in the presence or absence of BMEA.

Computer Modeling. The role of hydrophobic interactions in the binding of the above anthracene probes was evaluated in computational studies. Attempts were made to correlate the intrinsic binding constants of the anthracene derivatives with the octanol−water partition coefficient (Log *P*, where *P* = [solute in octanol]/[solute in water]). This coefficient is a good predictor of the hydrophobicity, and the partition coefficients are calculated by ClogP package of CaChe. Anthracene derivatives with larger number of hydroxyethyl functions have lower Log *P* values due to the additional OH groups present in the side chain. As expected, the increased number of hydroxyl functions decreased the Log *P* values.

A plot of Log *P* values against the binding constants of anthracene probes is shown in Figure 8. Note that the correlation is poor, and significant deviations in specific cases are clear. Only in the cases of AMAC and N-ET-AMAC did the binding affinity increase with Log *P* value, but, in all other cases, the binding affinities increased with decrease in Log *P*. The linear fit has a negative slope, and this strongly suggests that affinity decreases with increased hydrophobicity. The binding constant does not increase with hydrophobicity. Therefore, other interactions play a strong role in determining the overall binding affinities of these molecules.

Given the fact that these probes are closely related to each other, the binding should be related to common structural features such as hydrophobicity, the net charge on the probe, or the number of H-bonding/hydroxyethyl groups present on the ligand. Because hydrophobicity does not appear to control binding, and affinity increases in a substantial manner, there should be other major contributors to the binding.

A plot of binding constants against the number of hydroxyethyl groups indicated a strong linear correlation (Figure 9). The plot consisted of five data points, including N-Et-AMAC and AMAC, and the linear fit to the data is excellent. The positive slope indicates that the binding constant increases as a function of the number of hydroxyethyl groups, and the slope gives the contribution of each hydroxyethyl group to the binding. This works out to be $\Delta K_{binding}$ of 4×10^5 M^{-1} per hydroxyethyl group. This is the first demonstration of such a strong correlation between the DNA binding affinities and the number of hydroxyethyl functions present on the probe.

Note that N-Et-AMAC serves as an excellent control in the above plot because this probe is similar in structure to MEA but lacks the single hydroxyl group. The intrinsic binding constant of MEA (5.5×10^5 M^{-1}) is approximately 6 times larger than the binding constant of N-Et-AMAC (0.88×10^5 M^{-1}). Thus, addition of a single hydroxyl group has a profound

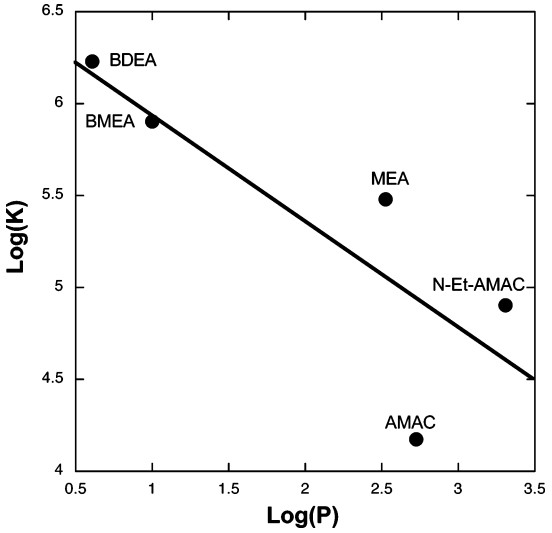

Figure 8. The plot of Log *K* versus Log *P* for the anthryl probes (the acronyms are defined in Chart 2). The solid line represents a linear fit to the data and indicated a poor correlation.

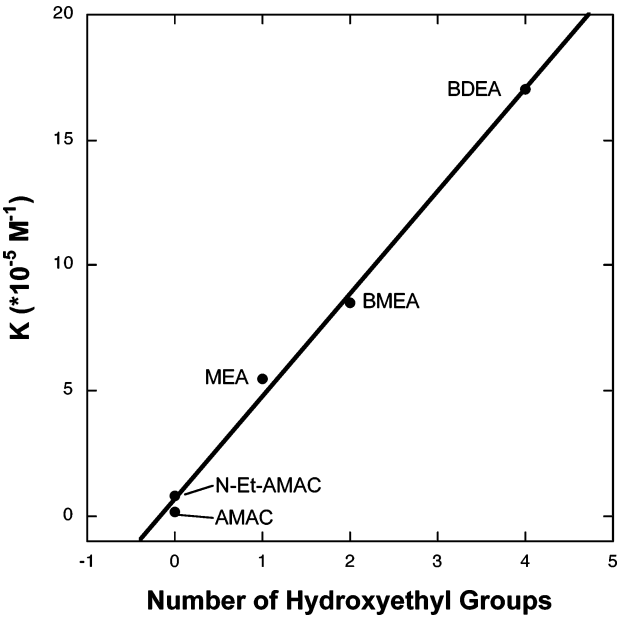

Figure 9. Plot of K_b as a function of the number of hydroxyethyl functions of the anthracene probes. The binding constants show a strong correlation with the number of hydroxyethyl groups present on the probe.

effect on the binding affinity. Even though the slope of the above plot includes contributions from the OH group as well as the CH_2–CH_2 unit, the contributions of CH_2–CH_2 to the binding affinity are either small or opposing to those of the OH group. A comparison of the affinities of AMAC and N-Et-AMAC (Figure 9) makes this point clear. The linear plot allows fair estimates of the DNA binding affinities of probes containing increasing number of hydroxyethyl functions and, perhaps, nonacidic OH groups.

Conclusions

Calorimetric, spectroscopic, and computational studies indicate that the anthracene probes bind to CT DNA with moderate to good affinities. The binding of both MEA and BMEA to CT DNA is exothermic (−3.4 to −5.5 kcal/mol), and binding is more exothermic with BMEA than with MEA. Because both probes are expected to be predominantly singly protonated at pH 7.2, this difference is likely due to the additional hydroxy-

ethyl group present in BMEA. Because the binding of AMAC or N-Et-AMAC to CT DNA is nearly thermoneutral, the enthalpy contribution due to each hydroxyethyl group can be deduced from these data.

The spectroscopic investigations indicate that the anthracene probes show bathochromic shifts ($\Delta E \approx 650$ cm^{-1}), extensive hypochromism (67−76%), strong positive CD peaks (300−450 nm region), and strong negative LD peaks in the 252 as well as the 300−450 nm region. These properties are also accompanied by helix stabilization ($\Delta T_m > 4-8$ °C) and significant increases in the enthalpy of helix denaturation ($\Delta\Delta H \approx 2.4-3.6$ kcal/mol).

These spectral and stability characteristics were identified with the intercalative binding of the anthracene probes but not groove binding.[15] Several anthracene probes bind via this mode, while there was also another binding mode that was associated with much weaker hypochromism (~30%), no shifts in the absorption spectral maxima, very weak ICD spectra in the 320−400 nm region, and no changes in the T_m of the ligand−DNA complex. Multiple binding modes are possible, but the spectral data indicate significant contributions of intercalation of both MEA and BMEA.

In case of BMEA, the DNA CD at 280 nm is reduced substantially. This reduction was attributed to the unwinding of the helix by the probe.[40] This interpretation was also supported by another example, BPA (R_1═R_2═CH_2−piperidine·2HCl), which also decreases the DNA CD at 280 nm to a significant extent. Therefore, we expect that intercalation of BMEA contributes to significant unwinding of the helix while intercalation of MEA is partial and does not unwind the helix substantially.

The linear plot in Figure 9 shows a strong correlation, and it will be useful to predict the binding affinities of similar molecules with hydroxyethyl substituents. This correlation also implies that the binding free energy varies nonlinearly among this set of molecules, and the underlying reasons for this behavior will be investigated in future studies. Meanwhile, the strong linear correlation and the slope of 4×10^5 M^{-1} per hydroxyethyl group are useful in the design of high-affinity DNA binding ligands.

Acknowledgment. C.V.K. thanks the National Science Foundation (DMR-0300631) for the financial support of this work.

Supporting Information Available: This material is available free of charge via the Internet at http://pubs.acs.org.

References and Notes

(1) Moser, H. E.; Dervan, P. B. *Science* **1987**, *238*, 645−650. Helene, C.; Thuong, N. T.; Saison-Behmoaras, T.; Francois, J. C. *Trends Biotechnol.* **1989**, *7*, 310−15.

(2) Neidle, S. *Nat. Prod. Rep.* **2001**, *18*, 297−309.

(3) Pilch, D. S.; Poklar, N.; Gelfand, C. A.; Law, S. M.; Breslauer, K. J.; Baird, E. E.; Dervan, P. B. *Proc. Natl. Acad. Sci. U.S.A.* **1996**, *93*, 8306−8311.

(4) Kimura, E.; Ikeda, T.; Shionoya, M. *Pure Appl. Chem.* **1997**, *69*, 2187. Wemmer, D. E.; Dervan, P. B. *Curr. Opin. Struct. Biol.* **1997**, *7*, 355. Trauger, J. W.; Baird, E. E.; Dervan, P. B. *Nature* **1997**, *382*, 559.

(5) (a) Tanious, F. A.; Jenkins, T. C.; Neidle, S.; Wilson, W. D. *Biochemistry* **1992**, *31*, 11632−11640. (b) Anthraquinone derivatives are well-known antitumor agents, see: Zee-Cheng, R. K. Y.; Cheng, C. C. *J. Med. Chem.* **1978**, *21*, 291. (c) Cheng, C. C.; Zee-Cheng, R. K. Y. In *Progress in Medicinal Chemistry*; Ellis, G. P., West, G. B., Eds.; Elsevier: Amsterdam, 1983.

(6) Carter, S. K.; Rall, D.; Schein, P.; Davis, R. D.; Wood, H. B.; Engle, R.; Davignon, J. P.; Venditti, J. M.; Schepartz, S. A.; Murray, B. R.; Zubrod, C. G. *Psuedourea*; National Cancer Chemotherapy Institute Clinical Brochure No. NSC56054, p 2.

(7) Pittillo, R. F.; Woolley, C. *Appl. Microbiol.* **1969**, *18*, 519−521.

(8) Becker, H. C.; Norden, B. *J. Am. Chem. Soc.* **1999**, *121*, 11947−11952.

(9) Wilson, W. D.; Tanious, F. A.; Watson, R. A.; Barton, H. J.; Strekowska, A.; Harden, D. B.; Strekowski, L. *Biochemistry* **1989**, *28*, 1984−1992. Wunz, T. P.; Dorr, R. T.; Alberts, D. S.; Tunget, C. L.; Einspahr, J.; Milton, S.; Remers, W. A. *J. Med. Chem.* **1987**, *30*, 1313−1321.

(10) Kumar, C. V.; Asuncion, E. H. *J. Am. Chem. Soc.* **1993**, *115*, 8547−8553.

(11) Kumar, C. V.; Asuncion, E. H. *Chem. Commun.* **1992**, 470−472. Rodger, A.; Taylor, S.; Adlam, G.; Blagbrough, I. S.; Haworth, I. S. *Bioorg. Med. Chem.* **1995**, *3*, 861.

(12) Kumar, C. V.; Tan, W. B.; Betts, P. W. *J. Inorg. Biochem.* **1997**, *68*, 177−181.

(13) Rodger, A. *Methods Enzymol.* **1993**, *226*, 232−258. Norden, B.; Kubista, M.; Kurucsev, T. *Q. Rev. Biophys.* **1992**, *25*, 51−171.

(14) Kumar, C. V.; Asuncion, E. H.; Tan, W. B. *Tetrahedron* **2000**, *56*, 7027−7040. Modukuru, N. K.; Snow, K. J.; Perrin, B. S., Jr.; Thota, J.; Kumar, C. V. *J. Phys. Chem. B* **2005**, *109*, 11810−11818. Modukuru, N. K.; Snow, K. J.; Perrin, B. S., Jr.; Bhambhani, A.; Duff, M.; Kumar, C. V. *J. Photochem. Photobiol., A* **2006**, *177*, 43−54.

(15) Tan, W. B.; Bhambhani, A.; Duff, M. R.; Rodger, A.; Kumar, C. V. *Photochem. Photobiol.* **2006**, *82*, 20−30.

(16) Robillard, M. S.; Galanski, M.; Zimmermann, W.; Keppler, B. K.; Reedijk, J. *J. Inorg. Biochem.* **2002**, *88*, 254−259. Zee-Cheng, R. K. Y.; Podrebarac, E. G.; Menon, C. S.; Cheng, C. C. *J. Med. Chem.* **1979**, *22*, 501−505.

(17) Maniatis, T.; Fritsch, E. F.; Sambrook, J. *Molecular Cloning: A Laboratory Manual*; Cold Spring Harbor: New York, 1982; p 458.

(18) Wang, C.; Delcros, J. G.; Biggerstaff, J.; Phanstiel, O. *J. Med. Chem.* **2003**, *46*, 2663−2671.

(19) Wunz, T. P.; Dorr, R. T.; Alberts, D. S.; Tunget, C. L.; Einspahr, J.; Milton, S.; Remers, W. A. *J. Med. Chem.* **1987**, *30*, 1313−1321.

(20) Breslauer, K. J.; Freire, E.; Straume, M. *Methods Enzymol.* **1992**, *211*, 533. Sturtevant, J. M. *Annu. Rev. Biochem.* **1987**, *38*, 463−88.

(21) McGhee, J. D.; von Hippel, P. H. *J. Mol. Biol.* **1974**, *86*, 469−486.

(22) Rodger, A. Linear Dichroism. In *Methods in Enzymology*; 1993; Vol. 226, pp 232−258.

(23) Refer for the partial specific molar volume of CT DNA: Durchschlag, H., Hinz, H. J., Eds. *Thermodynamic Data for Biochemistry and Biotechnology*; Springer-Verlag: New York, 1986.

(24) Doty, P.; McGill, B. B.; Rice, A. A. *Proc. Natl. Acad. Sci. U.S.A.* **1958**, *44*, 432.

(25) (a) Naga, K. M.; Snow, K. J.; Perrin, B. S.; Thota, J.; Kumar, C. V. *J. Phys. Chem. B* **2005**, *109*, 11810−11818. (b) Modukuru, N. K.; Snow, K. J.; Perrin, B. S., Jr.; Bhambhani, A.; Duff, M.; Kumar, C. V. *J. Photochem. Photobiol., A* **2006**, *177*, 43−54. (c) Tan, W. B.; Bhambhani, A.; Duff, M. R.; Rodger, A.; Kumar, C. V. *Photochem. Photobiol.* **2006**, *82*, 20−30.

(26) Long, E. C.; Barton, J. K. *Acc. Chem. Res.* **1990**, *23*, 271.

(27) Reinert, K.-E. *J. Mol. Biol.* **1972**, *72*, 593.

(28) Bisell, R. A.; Calle, E.; de Silva, A. P.; de Silva, S. A.; Gunaratne, H. Q. N.; Habib-Kiwan, J.-L.; Peiris, S. L. A.; Rupasinghe, R. A. D. D.; Samarasinghe, T. K. S. D.; Sandanayake, K. R. A. S.; Soumillion, J.-P. *J. Chem. Soc., Perkin Trans. 2* **1992**, *9*, 1559−1564.

(29) Ismail, M. A.; Sanders, K. J.; Fennell, G. C.; Latham, H. C.; Wormell, P.; Rodger, A. *Biopolymers* **1998**, *46*, 127−143.

(30) Ardhammar, M.; Norden, B.; Kurucsev, T. DNA−Drug Interactions. In *Circular Dichroism*, 2nd ed.; Berova, N., Nakanishi, K., Woody, R. W., Eds.; Wiley−VCH: New York, 2000; pp 741−768. Lyng, R.; Hard, T.; Norden, B. *Biopolymers* **1987**, *26*, 1327.

(31) Lyng, R.; Hard, T.; Norden, B. *Biopolymers* **1987**, *26*, 1327−1345.

(32) Rodger, A.; Norden, B. *Circular Dichroism and Linear Dichroism*; Oxford University Press: Oxford, UK, 1997; pp 2−8.

(33) Rodger, A.; Blagbrough, I. S.; Adlam, G.; Carpenter, M. L. *Biopolymers* **1994**, *34*, 1583. Meistermann, I.; Parkinson, A.; Vidler, D. S.; Haworth, I. S. *Chirality* **2000**, *12*, 221. Rodger, A.; Parkinson, A.; Best, S. *Eur. J. Inorg. Chem.* **2001**, *9*, 2311.

(34) Klump, H. In *Biochemical Thermodynamics*; Jones, M. N., Ed.; Elsevier: Amsterdam, 1988; p 100.

(35) (a)Klump, H. *Ber. Bunsen-Ges. Phys. Chem.* **1987**, *91*, 2018. (b) Klump, H.; Herzog, K. *Ber. Bunsen-Ges. Phys. Chem.* **1984**, *88*, 20.

(36) Kurnit, D.; Shafit, B.; Maio, J. *J. Mol. Biol.* **1973**, *81*, 273.

(37) Petraccone; et al. *Thermochim. Acta* **2004**, *418*, 47−52.

(38) (a) Berman, M, H.; Young, P. R. *Ann. Rev. Biophys. Bioeng.* **1981**, *10*, 87−114. (b) Leng, F.; Chaires, J. B.; Waring, M. J. *Nucleic Acids Res.* **2003**, *31*, 6191−6197. (c) Leng, F.; Priebe, W.; Chaires, J. B. *Biochemistry* **1998**, *37*, 1743−1753.

(39) Perrin, D. D.; Dempsey, B. *Buffers for pH and Metal Ion Control*; Chapman and Hall Laboratory Manuals: London, 1974.

(40) Lyng, R.; Hard, T.; Norden, B. *Biopolymers* **1987**, *26*, 1327−1345.